


Review

Rolling Contact Fatigue-Related Microstructural Alterations in Bearing Steels: A Brief Review

Hongxiang Yin ¹, Yi Wu ¹, Dan Liu ¹, Pengpai Zhang ¹, Guanzhen Zhang ¹ and Hanwei Fu ^{2,*} 

¹ Metal and Chemistry Research Institute, China Academy of Railway Sciences Corporation Limited, Beijing 100081, China; yhx0616@rails.cn (H.Y.); wuyi930@rails.cn (Y.W.); liudanjh@rails.cn (D.L.); zhangpp@rails.cn (P.Z.); zhangguanzhen@rails.cn (G.Z.)

² School of Materials Science and Engineering, Beihang University, Beijing 100191, China

* Correspondence: fuhanwei@buaa.edu.cn

Abstract: Bearings are vital components that are widely used in modern machinery. Although usually manufactured with high-strength steels, bearings still suffer from rolling contact fatigue where unique microstructural alterations take place beneath the contact surface as a result of the complex stress state. Studying these microstructural alterations is a hot research topic with many efforts in recent decades. In this respect, the key information regarding four major types of microstructural alterations, white etching areas/white etching cracks, dark etching regions, white etching bands and light etching regions is reviewed regarding the phenomenology and formation mechanisms. Then, classical and state-of-the-art models are established to predict their formation and are summarised and evaluated. Based on the current research progress, several key questions and paradoxes for each type of microstructural alteration are raised, suggesting possible research directions in this field.

Keywords: bearing steels; rolling contact fatigue; white etching areas; white etching cracks; white etching matter; dark etching regions; white etching bands; light etching regions



Citation: Yin, H.; Wu, Y.; Liu, D.; Zhang, P.; Zhang, G.; Fu, H. Rolling Contact Fatigue-Related Microstructural Alterations in Bearing Steels: A Brief Review. *Metals* **2022**, *12*, 910. <https://doi.org/10.3390/met12060910>

Academic Editors: Sergio Cicero and Sergio Arrieta

Received: 20 April 2022

Accepted: 20 May 2022

Published: 26 May 2022

Publisher's Note: MDPI stays neutral with regard to jurisdictional claims in published maps and institutional affiliations.



Copyright: © 2022 by the authors. Licensee MDPI, Basel, Switzerland. This article is an open access article distributed under the terms and conditions of the Creative Commons Attribution (CC BY) license (<https://creativecommons.org/licenses/by/4.0/>).

1. Introduction

Rolling contact fatigue (RCF) is a special type of fatigue occurring in rotational mechanical components, such as bearings, which are made of high-strength steels [1]. RCF eventually leads to the failure of components in the form of material removal at contact surfaces [2]. The development of RCF takes place during service where the material experiences repeated contact loading. Ideally, bearings operating under appropriate conditions are not supposed to fail in service. However, the improper use of bearings, such as misalignment, loose fit, corrosion, and poor lubrication, may occur, resulting in overloading or damage to the material that eventually leads to RCF [2].

In this context, RCF is likely associated with the low cycle fatigue of material. Unlike conventional fatigue scenarios (uniaxial push/pull, torsion, rotating bending, etc.) with well-defined and simple stress states, the stress state under rolling contact is rather complex because contact bodies typically exhibit curved surfaces (for example, bearing races and balls) [3]. This consequently makes RCF complex, involving unique crack behaviour and material decay. The contact between curved surfaces is also referred to as Hertzian contact where the shear stress components peak at the subsurface [3,4]. Therefore, subsurface-induced RCF is the most frequently observed cause for bearing failures.

During the subsurface-induced RCF of bearing steels, various microstructural alterations are one of the most distinctive features taking place. These microstructural alterations include white etching areas (WEAs)/white etching cracks (WECs), dark etching regions (DERs), white etching bands (WEBs) and light etching regions (LERs), which are named after their colors in contrast to the parent matrix under optical microscopy after etching with nital.

The occurrence of these microstructural features alters the mechanical properties of the material, exhibiting either material hardening or softening, creating interfaces that may facilitate crack growth [5]. This can severely affect the bearing life. Figure 1 illustrates the appearance sequence of microstructural alterations at different stages of RCF. The fatigue index was proposed by Tanaka et al. [6] to quantify the severity of RCF. L_{10} and L_{50} represent fatigue lives with 10% and 50% probability failure, respectively.

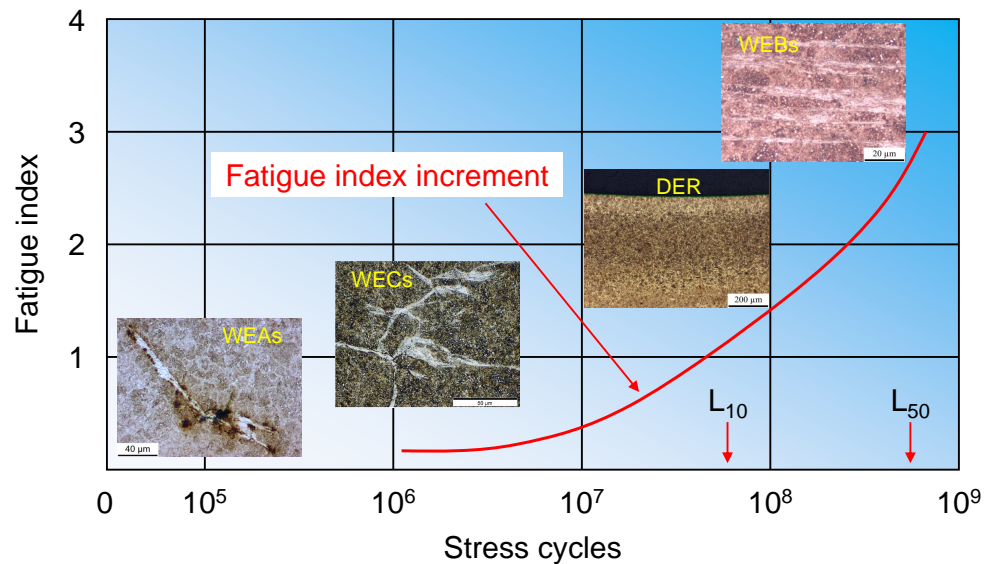


Figure 1. Appearance sequence of various microstructural alterations during the RCF of a 100Cr6 bearing steel. The increments of the fatigue index were based on the RCF test conducted with contact pressure of 3.4 GPa at room temperature. The image is drawn by referring to [7]. The image of WEAs was adapted from ref. [8], and the image of WECs was adapted from ref. [9]. Copyright 2019 Springer Nature; the image of DERs was an unpublished image, and the image of WEBs was adapted from ref. [10].

Since the first observation in 1946 [11], extensive efforts have been made to study RCF-related microstructural alterations in bearing steels. The phenomenology of these microstructural features is rather unique and complex, and their occurrence depends on both the bearing operation conditions and initial microstructure. They all exhibit the decay of the parent matrix, manifesting the instability of the microstructure as a result of RCF. Without understanding the nature and underlying physics of these microstructural alterations, it is impossible to accurately evaluate the performance of bearing steels in service.

Figure 2 shows the circumferential and axial sections of a bearing raceway where microstructural alterations are usually observed. According to the figure, the axial section is perpendicular to the over-rolling direction (ORD), while the circumferential section is parallel to the ORD below the centre of contact. The unique directionalities of some microstructural features can only be observed from the circumferential section. With the development of characterisation techniques in recent decades, these microstructural features have been observed from the micro-scale to the nano-scale and atomic scale [12].

Based on the observations, numerous mechanisms have been proposed to account for the formation process of these microstructural features. Nonetheless, rolling contact fatigue-induced microstructural alterations in bearing steels are still a hot research topic with a number of key problems unsolved. Moreover, modelling and predicting the formation of these microstructural alterations becomes crucial for the bearing industry where the reliability of material is highly demanded.

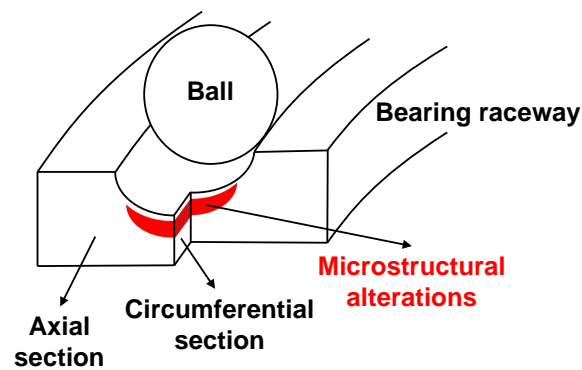


Figure 2. Sections of a bearing raceway where microstructural alterations are usually observed.

In this respect, this work presents a brief review of rolling contact fatigue-related microstructural alterations in bearing steels. The phenomenology of various microstructural features is reviewed first to reveal their microstructural nature, along with the proposed formation mechanisms based on the experimental observations; then, the models established to predict the formation of these microstructural features are reviewed, summarising the available modelling tools in this field; finally, several unsolved questions in this field are raised with research directions suggested for future work.

2. Phenomenology and Formation Mechanisms

2.1. WEAs and WECs

As shown in Figure 3a, observing from the circumferential section of a rolling contact fatigued bearing inner race white etching areas (WEAs) are found adjacent to cracks initiated from hard phase particles in bearing steels, such as non-metallic inclusions (NMIs) [13] and carbides [14]. WEAs start to occur at relatively early stages of bearing life, after approximately $0.001L_{10}$ [7]. Typically, WEAs appear in a pair on both sides of a hard particle but on only one side of each crack. Owing to such a unique shape, WEAs are also referred to as butterflies [15].

The typical inclination angle of butterflies is approximately 45° with respect to the over-rolling direction although some studies [14] show that, by increasing the contact pressure, this angle can be reduced. Nonetheless, this inclination angle makes researchers believe that the maximum shear stress (τ_{45}) is responsible for the occurrence of WEAs [15]. In addition, the occurrence of WEAs is dependent upon the over-rolling direction.

As proven experimentally, when the over-rolling direction was reversed, another pair of WEAs appeared symmetrically [16]. This indicates that surface traction may play a role in terms of butterfly formation. The subsurface stress state calculated for a pure rolling condition is unable to explain the asymmetric appearance of WEAs with a given over-rolling direction. As suggested by Hills et al. [17], the stress state under Hertzian contact can be altered by slipping, which may further affect the multi-axial initiation of fatigue cracks at inclusions as analysed by Alfredsson and Olsson [18].

WEAs can be formed in martensitic [19], bainitic [20] and case-hardened bearing steels [21], and the microstructure of WEAs is distinctly different from the parent matrix. Currently, the white microstructure decorating cracks is generally referred to as white etching matter (WEM) [22], not only for the case of butterflies but also for white etching cracks (WECs). As revealed by electron backscatter diffraction (EBSD) [23] and transmission electron microscopy (TEM) [15,24,25], WEA microstructure consists of ferritic grains/dislocation cells with their size ranging from 5 to 200 nm (Figure 3b).

The selected area electron diffraction from WEA microstructure exhibited typical diffraction rings that indicated very small crystal size [24,26]. Such fine microstructure is the cause for the white etching contrast. The grain/dislocation cell size distribution was found to be location dependent. As a WEA/butterfly wing consists of two boundaries, one being a crack and the other being a feathery interface between the WEA and the matrix, it

was found that the grain/dislocation cell size gradually increases with the distance away from the crack [19].

Nonetheless, the WEA microstructure is highly dislocated where the dislocation density was estimated by Grabulov et al. [15] to be 10^{16} – 10^{17} m^{-2} . Carbide dissolution was also detected during the formation of WEAs where some [15] argued partial dissolution and the others [24] argued complete dissolution. The extra carbon from the dissolving carbides is present in the solid solution, and given the limited solubility, carbon in a ferrite WEA microstructure is therefore carbon supersaturated.

Three-dimensional atom probe tomography (APT) on the WEA microstructure (Figure 3c) showed that the solute carbon atoms were segregated at dislocation cell walls leaving carbon-depleted cell interiors [26–28]. It is generally believed that the segregated carbon stabilises cell walls such that the nano-sized structure is maintained and the grain size in WEAs was found to be inversely proportional to the local carbon content [29]. However, the overall carbon content in WEAs decreases during their formation. This phenomenon was first reported by Kang et al. [26] who conducted APT investigation on WEAs and found the total carbon content in WEAs to be lower than the nominated composition; however, they attributed such observations to the limited resolution in terms of the carbon ions in APT.

Later, Curd et al. [30] confirmed the carbon loss in WEAs with an electron probe micro analyser. Regarding this, the latest explanation is that the lost carbon is present at the crack surface in the form of graphite [31]. The WEA microstructure exhibits significant material hardening. Micro-indentation testing showed that the hardness of the WEA microstructure can be as high as 1000 HV [24]. It is believed that such high hardness stems from both dislocation hardening and solid-solution hardening from solute carbon atoms [19].

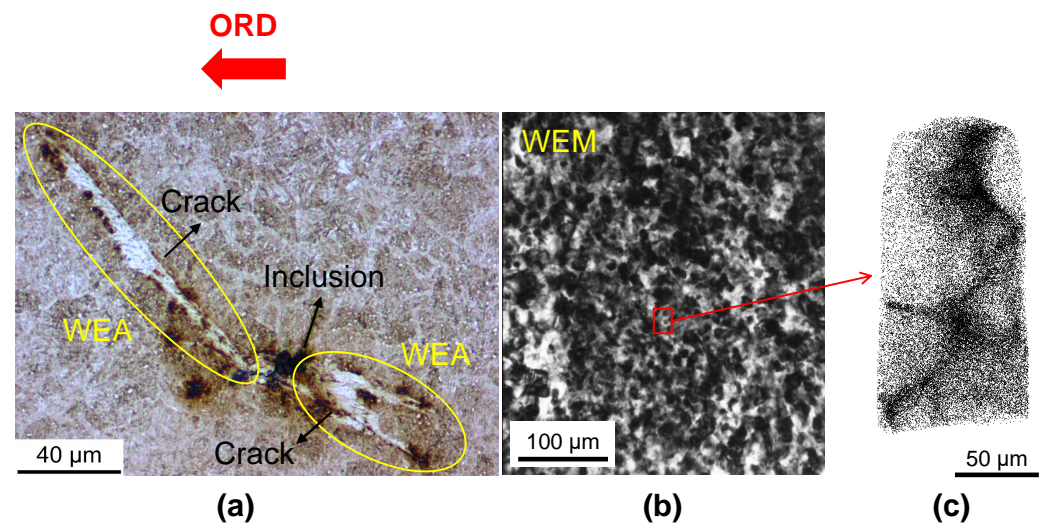


Figure 3. Formation of WEAs. (a) Optical image of a pair of WEAs initiated from an inclusion. The image was adapted from ref. [8]. (b) Unpublished TEM image of the microstructure inside WEM. (c) APT result of carbon distribution in a dislocation cell in WEM. The image was adapted from ref. [8].

Similar to butterflies, white etching cracks (WECs) are also cracks decorated by white etching matter (WEM), the microstructure of which is identical to that of WEAs; however, WECs appear as crack networks that extend within a larger region at the subsurface [32]. WECs have drawn significant research attention as they account for the majority of unpredicted failures of bearing components, sometimes leading to ‘premature failures’ [33,34]. Such unpredicted bearing failures are costly in the wind turbine, automotive and other industry gearboxes [35]. The understanding of the formation mechanism of WECs and the possible measures to suppress their formation are highly demanded by bearing manufacturers.

In this respect, Evans et al. [36–38] conducted systematic characterisation on WECs in wind turbine bearings and discovered intense interactions between WECs and certain types of NMIs. Hence, they argued that WECs are extended butterflies. This indicates that controlling the inclusion microstructure of bearing steels is crucial for bearing life. The most frequently found butterfly initiators in 100Cr6 bearing steel are Al_2O_3 [15] and MnS particles whereas in M50 bearing steel, although the cleanliness is extremely high after double vacuum metallurgy, butterflies still arise from large carbide particles [14].

Referring to Grabulov et al. [23], who investigated the interface between Al_2O_3 particles and the steel matrix, interface debonding that yields sufficient rubbing during rolling contact was argued to be the key to initiating WEM formation. This explains why WEAs were never found adjacent to Fe_3C particles in 100Cr6 bearing steel, which exhibits good coherence with the steel matrix whilst the carbide particles in M50 bearing steel (mainly MC and M_2C) [21] exhibiting bad coherence with the steel matrix act as butterfly initiators.

The formation mechanism of the white etching microstructure has been extensively studied. The main microstructural features of WEM—high dislocation density, ultra fine grains, carbide deformation and dissolution—strongly indicate the occurrence of severe plastic deformation (SPD). The origin of such a high degree of plastic strain is generally believed to be the rubbing of crack surfaces [21,39]. This owes to the unique stress history under Hertzian contact where the subsurface stress components continue alternating in direction and magnitude with the ball over-rolling [4].

It was observed that the surfaces of the main branch of a WEC that had been heavily rubbed were extremely smoothed, whereas the newly formed leading branches still exhibited a kink-type morphology [40]. Furthermore, the non-uniform grain size distribution in WEM indicates a stress/strain gradient with respect to the distance from the crack [19]. The thickness of well-developed WEM is typically a few microns, suggesting the limit of influence from crack surface rubbing. As suggested by many researchers [24,29], the refined grains in WEM are formed by a multi-stage mechanism.

Generally speaking, dislocation multiplication first takes place; the forest dislocations cluster to form dislocation cell walls with a low energy configuration; then, the cellular structure further develops by consuming the dislocations in cell interiors and the compacting of cell walls; and finally, the cell walls may develop into grain boundaries with large misorientations [19]. Accompanying this whole process of plastic strain accommodation is the decomposition of carbide particles with the excess carbon atoms migrating towards the cell walls.

According to Fu et al. [8], such carbon migration is assisted by gliding dislocations. Nonetheless, the amorphization in WEM is a complex process that may involve multiple mechanisms, considering some other microstructural features observed in WEM, such as crack traces and micro cavities [41]. Morsdorf et al. [40] also confirmed the presence of a material flow during WEM formation using Cr as an indicator element. The formation of WEM was once believed to be a symptom of crack growth that has no influence to the bearing life [22]; however, increasingly studies [30,31,42] have shown the mutual growth of cracks and WEM.

In addition, the WEM microstructure resembles that of white etching layers, which are often formed on repeatedly run rail surfaces. In white etching layers, the parent pearlitic matrix transforms into an ultrafine crystalline microstructure with significant carbide dissolution [43]. It is generally accepted [44,45] that the white etching layer microstructure is a result of repeated SPD caused by surface sliding, which may be similar to the rubbing of crack faces.

2.2. DERs

DERs are formed in rolling contact fatigue tested bearing steels under moderate and high contact pressures, exhibiting martensite decay [46].

A DER usually starts from a certain depth below the contact surface and then further extends along depth. Such distribution of DERs strongly indicates the influence from subsurface stress state under Hertzian contact. By comparing the depth range of DERs and the distribution of various stress components, most authors [47] argued that orthogonal shear stress was the responsible stress component, whilst some others [48] argued for the von-Mises stress component. This disagreement may be due to the differences in stress magnitude and rolling contact geometry in different studies. A DER is composed of dark patches dispersed in the matrix.

While the area fraction of dark patches varies along depth; with increasing depth, it first increases rapidly and then gradually decreases to zero. Such variation trends also agree with that of subsurface shear stresses. For a developing DER, with an increasing number of cycles, the area occupied by dark patches increases overall, and the depth range of the DER is widened (Figure 4a). The formation of DERs results in significant material softening [47,49,50]. The maximum softening extent can reach 150 HV in 100Cr6 bearing steel [49].

Nonetheless, at relatively high contact pressures (>4 GPa), a hardness increase was detected in DERs, which is due to the softening effect being outperformed by severe work hardening. TEM showed that the dark patches in DERs consist of ferrite. Given the low solubility of carbon in ferrite, the whereabouts of excess carbon becomes a key issue. Regarding this, the early hypothesis [46] was that carbon atoms were segregated at dislocations; however, the dislocation density required to accommodate such a large amount of carbon atoms was estimated to be impossibly high.

Later, Fu et al. [47] utilised APT to study the distribution of carbon in DERs (Figure 4b), finding that the solid solution was carbon depleted and that the pre-existing carbide precipitates were thickened. The decrease of carbon content in the solid solution explains the detected material softening in DERs while the thickening of carbide precipitates explains the origin of dark etching contrast as nital etchant mainly reveals carbide/matrix interfaces. Despite matrix decay, primary spherical carbide particles remain unaltered in DERs. The formation of globular and elongated grains was found in the DER microstructure by Smelova et al. [51] using EBSD, and they attributed this phenomenon to dynamic recrystallization.

A similar opinion was also proposed by Kang et al. [52] who observed a strong $\langle 111 \rangle$ // ND texture, which is typical for recrystallized body-centred-cubic alloys, in DERs. Given the low operation temperatures of RCF tests, the activation of dynamic recrystallisation becomes difficult where further theoretical justification by calculating the threshold conditions is required.

As the microstructure of DERs highly resembles tempered martensite, early studies postulated that subsurface shearing during RCF causes a localised heat rise [5], leading to the formation of DERs; however, this postulation lacks experimental evidence. The fact that the occurrence of DERs can be accelerated by either increasing the contact pressure or temperature indicates both mechanical and thermodynamic mechanisms operating during DER formation.

On the one hand, Bush et al. [49] found a threshold contact pressure under which DERs were never formed, and the stress magnitude corresponded to the onset of plastic flow in bearing steels; on the other hand, the microscopic observations suggest that carbon redistribution governs the formation of DERs. Following the above experimental results, Kang et al. [53] proposed a strain-tempering mechanism for DER formation, suggesting that, under RCF, carbon atoms in the solid solution are dragged by gliding dislocations in the form of Cottrell atmospheres [54] towards nano-sized carbide precipitates to thicken them.

The process of this strain-tempering mechanism was later modified by Fu et al. [47] and named dislocation-assisted carbon migration. It is noteworthy that, under this mechanism, the state of pre-existing carbide precipitates plays an essential role in DER formation. These

nano-sized carbide precipitates are formed during the tempering process of bearing steels, mainly of θ , ϵ and η types, and also referred to as transition carbides. For bearing steels tempered with a relatively low temperature and short time, transition carbides are usually not fully developed and tend to grow further.

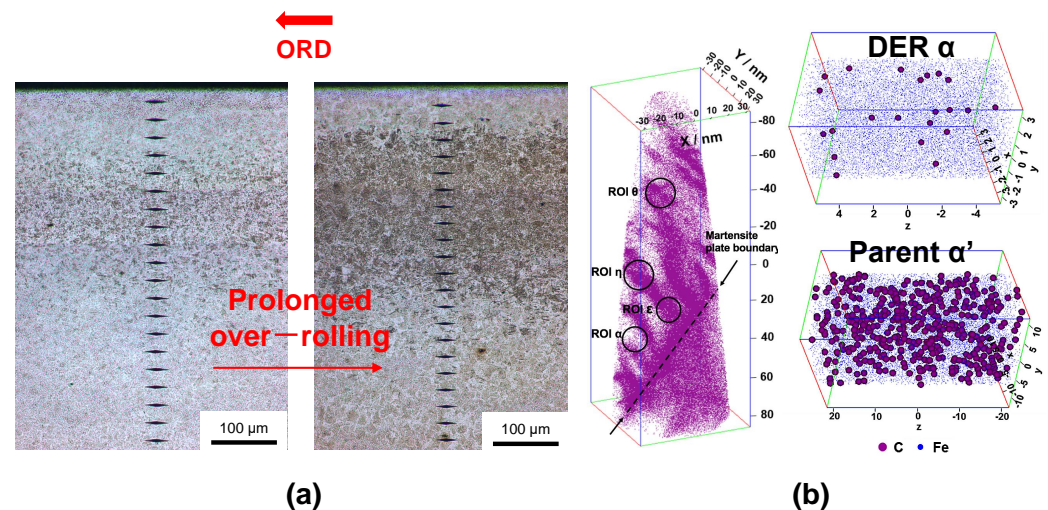


Figure 4. Formation of DERs. (a) Optical images showing the development of DERs in a circumferential section with prolonged over-rolling. The RCF tested was conducted on 100Cr6 bearing steel with a contact pressure of 3.3 GPa at 70 °C for 10^7 and 10^8 cycles, respectively. (b) APT investigation of DER microstructure. The images are adapted from ref. [47].

This provides the thermodynamic driving force for carbide thickening. The dislocation-assisted carbon flow provides the kinetics for the further growth of carbide precipitates during RCF. On the contrary, if transition carbides in bearing steels are fully developed, DERs may never appear despite the presence of dislocation-assisted carbon flow. This may be the reason why DERs were reported to be eliminated in bearing steels tempered with high temperature and long times [10,53,55].

2.3. WEBS

At the late stages of bearing life, WEBS start to appear. If a DER is formed in the first place, WEBS are found at the lower part of it; however, WEBS can also be formed in the absence of DERs [10]. By comparing the depth range of the WEB formation with the subsurface stress state, it is generally believed that the maximum shear stress [49] and von-Mises stress [56] are the main responsible stress components.

According to Figure 5a, observing from the circumferential section, WEBS are classified into two types: low angle bands (LABs) that are inclined about 30° to the contact surface and high angle bands (HABs) that are inclined about 80° to the contact surface. Observing from the axial section, WEBS are stripes parallel to the contact surface (Figure 5b). Hence, it can be expected that WEBS are plate-like in three dimensions [10,50]. During RCF, LABs always appear prior to HABs [5].

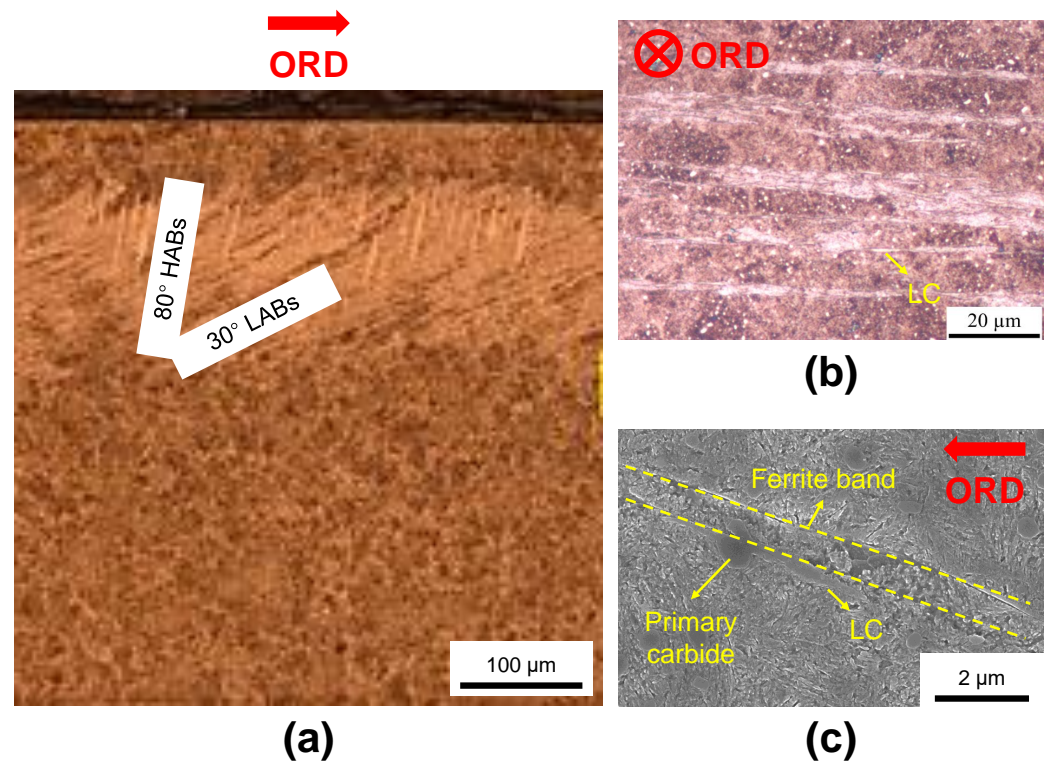


Figure 5. Formation of WEBS. (a) Optical image of LABs and HABs in the circumferential section (image adapted from ref. [57]). The RCF test was conducted with a contact pressure of 2.9 GPa for 3×10^9 cycles. (b) Optical image of LABs in axial section (image adapted from ref. [10]). (c) Unpublished SEM image of a LAB consisting of a ferrite band and a LC. A partially dissolved primary carbide can also be seen.

From both circumferential and axial sections, LABs are long and thin stripes. Fully developed LABs can reach 50 μm in length; however, their thickness usually saturates at 7–10 μm [58]. With an increasing number of cycles, the number density, formation depth range and average size of LABs all increase [10,59]. In most of the cases, the structure of LABs is unique, consisting of white bands and lenticular carbides (LCs) adjacent to them (Figure 5b,c).

Figure 6 is a TEM image of a LAB showing that the microstructure of the white bands is ferritic, exhibiting dislocation cells that are 100–200 nm in size. The composition of lenticular carbides was confirmed by Fu et al. [55] to be Fe_3C . No carbide precipitates can be found inside ferrite bands, indicative of carbide dissolution during LAB formation. Moreover, the hardness of ferrite bands is lower than the unaltered matrix [10] and even lower than the surrounding DERs [50].

Such hardness reduction is believed to stem from carbon depletion in ferrite bands. The outflow of carbon facilitates the precipitation of LCs. HABs, however, are formed on the top of fully developed LABs in a different direction, consisting of carbon-free ferritic grains and are about five-times thicker than LABs [60]. Although both appearing as white contrast, the microstructure of WEBS is distinctly different from that of WEM. The main difference is the whereabouts of carbon.

WEM with higher hardness than the parent matrix contains a high carbon content in the solid solution, whilst the ferrite bands in WEBS with significant hardness reduction are almost carbon free. Considering the stabilization effect of carbon on dislocation cells, this may explain why the grains in ferrite bands are much coarser [29]. Nonetheless, the rearrangement of dislocations in ferrite bands suggests plastic deformation [61]. Moreover, the growth of WEBS can dissolve primary carbide particles standing in their way (Figure 5c).

In 100Cr6 bearing steel, primary carbides contain Cr, and it was found that Cr released from dissolving was homogenised inside WEBS [51]. It is noteworthy that, in RCF tested M50 and M50-NiL bearing steels, although both LABs and HABs can appear, no LCs were ob-

served [62–64]. This may be because the carbides in these steels are too stable to decompose [21], and without carbon concentration, increases in the solid solution LCs are eliminated.

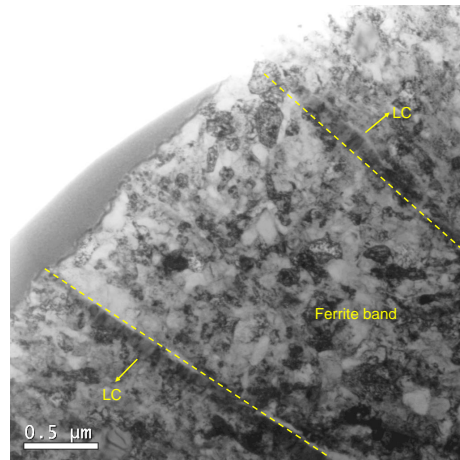


Figure 6. Unpublished TEM image of a lamella prepared by a focused ion beam of a LAB consisting of a ferrite band and LCs.

The formation mechanism of WEBs has been debated for decades. Early postulations [11,50] that WEBs are caused by local temperature rise can be rebutted by the finding of threshold stresses, which suggest a stress-induced mechanism [49]. Later, Bush et al. [49] proposed an intrusion–extrusion mechanism for WEB formation by referring to the intrusion–extrusion process of aluminium and argued LCs to be sheared primary carbide particles. However, the size of LCs is too large to stem from primary carbides alone, and given the detected carbon depletion in WEBs, carbon from ferrite bands must have participated the thickening of LCs.

Swahn et al. [46] suggested an energy increase at ferrite boundaries, promoting LC nucleation, while some [5] argued that a high density of dislocations at the ferrite boundaries provides favourable LC nucleation sites. In this respect, the driving force for such a carbon outflow and the associated kinetics become an issue.

Swahn et al. [46] emphasized the energy increase due to plastic deformation to be the driving force. Buchwald et al. [58] attributed the carbon-migration kinetics to both concentration gradient and pressure gradient. Becker [24] and Polonsky et al. [65] postulated diffusion-based mechanisms for LC formation considering carbon supersaturation in ferrite bands caused by carbon release from Cottrell atmospheres.

The latest explanation to LC formation was proposed by Fu et al. [55] arguing that carbon atoms in ferrite bands are transported by gliding dislocations toward LCs. Nonetheless, WEBs are likely stress-induced. The growth of LCs may act as an indicator for LAB development [55,66]; however, LCs are not a requirement for WEB formation, given the observed WEBs in absence of LCs in M50 bearing steel [62–64].

2.4. LERs

LERs can be found only in bearing steels for aerospace high temperature applications, such as M50 (through hardened) [62,63,67] and M50-NiL (case-hardened) [64,68]. Due to the special application scenario of these steels, only a few studies [14,62–64,67–69] have been reported on LERs. As shown in Figure 7, LERs manifest the decay of parent martensite consisting of light etching patches dispersed in the matrix.

The depth range of LERs is similar to that of DERs, and thus orthogonal shear stress can be regarded as the responsible stress component as well. With increasing numbers of stress cycles, LERs become larger in size and denser in white contrast. Contrary to DERs that cause material softening, LERs exhibit material hardening. The occurrence and development of LERs can be effectively promoted by increasing the contact pressure [62].

Although the influence of temperature on LERs has not been studied, it can be concluded that high temperature is a favourable condition for LER formation given that almost

all reported LERs were observed with RCF testing temperatures higher than 100 °C [62,63] whilst the M50 specimens tested with high contact pressure and room temperature did not show LERs [14]. The characterisation of LERs is currently limited at the microscale, and the detailed microstructure of LER is still unclear. Pritz et al. [67] conducted EBSD investigation on LERs but obtained poor resolution, although a likely preferred grain orientation of (111) was found.

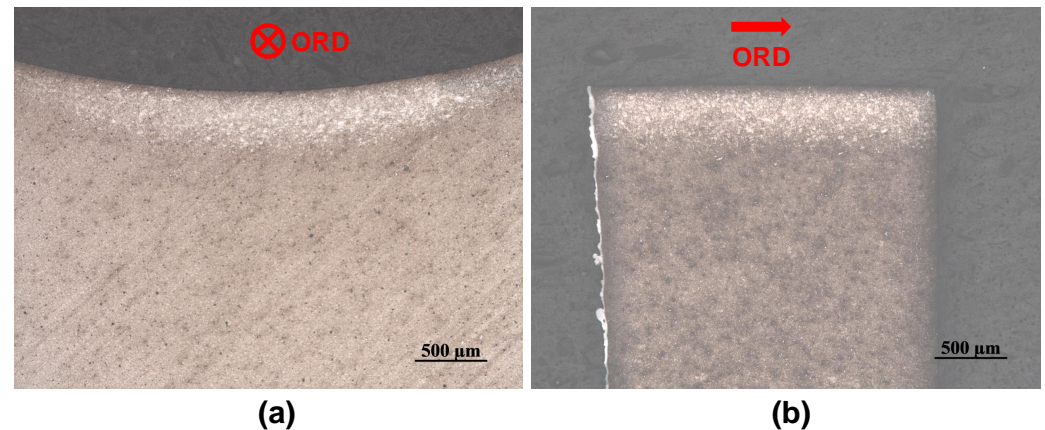


Figure 7. Formation of LERs in M50 bearing steel observed from axial section (a) and circumferential section (b). The RCF test was conducted with contact pressure of 2.95 GPa at 127 °C for 1.3×10^9 cycles. The images were unpublished.

The formation mechanism of LERs is not well understood yet. In the reported studies so far, LERs were attributed to accumulated damage and residual stress [69]. Nonetheless, the white contrast is indicative of microstructural refinement, likely with dislocation rearrangement or carbon redistribution. Therefore, more characterisation work at the nano-scale and the atomic-scale is demanded to reveal the underlying physics during LER formation.

2.5. Influence of Hydrogen

High-strength steels, such as bearing steels are prone to hydrogen embrittlement. The influence of hydrogen on the RCF-related microstructural alterations has been extensively studied as well. Experimental evidence has shown that hydrogen is no doubt an accelerator for the occurrence of WEAs/WECs [36,70–74], DERs [73,75] and WEBs [75,76]. Such accelerating effects of hydrogen were usually attributed to hydrogen-enhanced localised plasticity (HELP) [77] and hydrogen-promoted crack growth [71]. Except for intended hydrogen charging in some RCF tests [70,71], the ingress of hydrogen for bearings during use mainly results from the decomposition of lubricant.

In addition, attention is mainly focused on determining whether hydrogen is the root cause for WEM formation [78]. In most of the cases [73,79,80], hydrogen was found to alter the plastic response of bearing steels and consequently accelerate WEM formation. However, direct evidence showing the correlation between hydrogen and WEA/WEC initiation is still absent. Nevertheless, a number of studies [81–83] suggest that WECs can be eliminated with certain lubricant compositions and relate this to the resultant hydrogen concentration in the material.

3. Predicting Approaches

Considering the reliability and safety of bearing components, predicting the formation of the RCF-related microstructural alterations is an important but difficult task. As these microstructural alterations are governed by both external and internal factors, with the former being the rolling contact conditions and the latter being the initial microstructure. The established models should incorporate all these factors as input parameters. Moreover,

although RCF is somehow related to the low cycle fatigue of material, the modelling of these microstructural features is beyond the framework of low cycle fatigue.

Technically, the modelling strategies presented in the literature can be roughly summarised as numerical modelling that focuses on describing physical processes with mathematical derivation. However, it should be noted that disagreements still exist on the formation mechanisms of some microstructural alterations [12], leading to various models based upon different grounds. In this section, predicting models for three major types of microstructural alterations, WEAs, DERs and WEBs, are reviewed and evaluated. No model has been reported for LERs.

3.1. WEA Models

WEAs or butterflies were modelled at various scales. At the microscale, Rydel et al. [14] statistically studied the distribution and size of butterflies accompanying carbides in RCF tested M50 bearing steel and proposed an empirical butterfly nucleation and growth model. According to the model, the number of stress cycles for a butterfly to nucleate (N_i) is expressed as:

$$N_i = \frac{c}{\sigma_{vM} - \sigma_i} \quad (1)$$

where c is the total accumulated damage required for nucleating a butterfly, σ_{vM} is the local von Mises stress and σ_i is the threshold stress for butterfly nucleation, which follows a normal distribution with a given number of carbides. Subsequently, the length of an individual butterfly (L_i) after a certain number of cycles (N) is given by:

$$L_i = b_i \ln(N - N_i) \quad (2)$$

where b_i is the individual butterfly growth rate proportional to the size of the associated carbide. The carbide size was proposed to follow a log-normal distribution. Due to the statistical nature of the proposed model, it only works for a collection of butterflies, and the fitting parameters used are highly dependent upon the parent microstructure. Furthermore, it should be noted that the number of cycles required to nucleate microcracks is also influenced by the presence of voids as suggested by Dogahe et al. [84]

At the nano scale, based on the APT observations that carbon atoms are segregated at dislocation cell walls in WEM, Fu et al. [8] employed the dislocation-assisted carbon migration mechanism to describe dislocation cell formation and to subsequently predict the occurrence of WEAs. The dislocation-assisted carbon migration mechanism was proposed by Fu et al. and first used to account for the evolution of LCs in WEBs [55]. This was later extended to describing the formation process of DERs [47] and finally applied to WEAs and summarised as a unified theory for rolling contact fatigue-induced microstructural alterations [8]. The underlying physics of the mechanism are introduced as follows.

Considering the initial martensitic microstructure of a bearing steel, carbon atoms tend to be segregated at dislocations in the form of Cottrell atmospheres [54]. Then, with the ball over-rolling on a raceway, the material experiences repetitive stress pulses with each one representing the advent of a ball at a certain point. Once the stress level exceeds the yield strength of the material, dislocation glide takes place where dislocations break out of their original carbon atmospheres and move to new positions. This dislocation movement is accomplished immediately within a stress pulse, and the time interval before the advent of the next stress pulse allows carbon atoms to catch up with the gliding dislocations, forming new Cottrell atmospheres.

This process is repeated during ball over-rolling and thus creates a carbon flux within the material. Such carbon migration is a combined result of plastic strain and carbon diffusion. Therefore, it can be expected that the higher the plastic strain, the longer the distance carbon atoms can migrate; and the higher the temperature, the greater the number of carbon atoms that can be transported. By referring to Cottrell atmosphere theory [54] and

the Orowan Equation [61], Fu et al. [8] gave the mathematical form of dislocation-assisted carbon flux (J_d) as:

$$J_d = \frac{\Delta\gamma\dot{N}}{b} \left[3 \left(\frac{\pi}{2} \right)^3 \left(\frac{AD}{kTN} \right)^{\frac{2}{3}} C_V^I \right] \quad (3)$$

where $\Delta\gamma$ is the amplitude of the plastic shear strain within each stress pulse, \dot{N} is the stress cycle frequency, b is the magnitude of the Burgers vector, A is a constant evaluating the interaction between a dislocation and a carbon atom, D is the diffusion coefficient of carbon in martensite, k is the Boltzmann constant, T is the temperature, and C_V^I is the background carbon concentration.

In the case of WEM, it was postulated that dislocation cell formation is dominated by carbon migration from cell interiors to cell walls. The whole process can be quantitatively described via the carbon flux equilibrium and carbon mass conservation as:

$$\frac{dh_c}{dN} (C_V^w - C_V^i) \dot{N} = J_d \quad (4)$$

$$r_c^3 C_V^0 = (r_c - h_c)^3 C_V^i + [r_c^3 - (r_c - h_c)^3] C_V^w \quad (5)$$

where h_c is the thickness of the cell wall; N is the number of cycles; C_V^w and C_V^i are the carbon concentrations in cell walls and cell interiors, respectively; C_V^0 is the overall carbon concentration of the steel; and r_c is the radius of dislocation cells. Note that C_V^I in J_d here is C_V^i . By solving Equations (4) and (5), a degree of completion curve for dislocation cell formation can be plotted from which the number of stress cycles required for 100% dislocation cell completion can be indexed and is regarded as when WEAs appear. By further assuming that WEA appearance usually happens at $0.001L_{10}$ [7], RCF life can be estimated. The proposed WEA formation model was validated by the experimental results from various studies [7,8,85].

Moreover, the model by Fu et al. was recently extended by Liang et al. [71] to account for the acceleration effect of hydrogen on WEA formation. Hydrogen-enhanced localised plasticity was incorporated into the model via enhanced $\Delta\gamma$. The model was proven to be able to replicate numerous experimental observations reported in the literature.

3.2. DER Models

Based on the postulation that DERs are formed by carbide precipitate growth with the assistance of gliding dislocations, Kang et al. [53] proposed a strain tempering model to predict hardness reduction in DERs with the first DER formation model. However, the model yields the prediction that, with increasing contact pressure, DER formation tends to be retarded, which contradicts experimental observations.

This is due to the model assuming a continuous dislocation movement manner where the carbon transportation capability of dislocations is negatively correlated with the dislocation speed. In this respect, Fu et al. [47] employed dislocation-assisted carbon migration, which takes into consideration the stress pulses occurring during rolling contact, to predict the development of DERs based on the same DER formation mechanism. The core equations of the model were given as:

$$\frac{dr_p}{dN} (C_V^p - C_V^m) \dot{N} = J_d \quad (6)$$

$$l_p C_V^0 = 2r_p C_V^p + (l_p - 2r_p) C_V^m \quad (7)$$

where r_p is the radius of carbide precipitates, l_p is the spacing distance between carbide precipitates, C_V^p and C_V^m are carbon concentrations in carbide precipitates and in the matrix, respectively. Note that C_V^I in J_d in this case is C_V^m . By solving Equations (6) and (7), the evolution of the carbon content in the matrix can be quantitatively described, which is subsequently correlated with the development of DERs and the corresponding hardness

reduction. The model was compared against the reported observations in the literature over the past 70 years with relatively good agreement obtained.

The DER formation model by Fu et al. was recently employed in various studies, with some obtaining good predictions while some others argued discrepancies. Kang et al. [86] incorporated the model into a crystal plasticity and continuum damage mechanics model for RCF simulation and produced accurate predictions of the DER distribution and lifespan of 52,100 bearing steel. Kang et al. [52] employed the model to predict the evolution of DERs in a 0.57C-bearing steel tested with a flat washer, obtaining good predictions. On the other hand, Abdullah et al. [48] compared the experimental observations from 100Cr6 bearing steel after a number of RCF tests with various contact pressures and temperatures with the calculation results of the model and argued overprediction. The effects of thermal diffusion and cyclic plasticity were emphasized.

3.3. WEB Models

Despite numerous key questions remaining unanswered for WEB formation, a great deal of efforts were made regarding the explanation of the most striking phenomenon in LABs—the formation of LCs. As it is widely accepted that the carbon participation in the thickening of LCs is from their adjacent ferrite band, various LAB formation models have been proposed based on different carbon outflow mechanisms.

Buchwald et al. [58] argued that the presence of both a carbon concentration gradient and pressure gradient leads to the precipitation of LCs, where the former stems from the dissolution of pre-existing carbides and the latter stems from localised deformation in a confined volume. Based on the proposed mechanism, the LC thickening rate was given as:

$$\frac{dl_{LC}}{dt} = \frac{D}{C_V^\theta - C_V^0} \left(\nabla C + \frac{C_V^0}{RT} \nabla v \right) \quad (8)$$

where l_{LC} is the thickness of LCs, t is the operation time, C_V^θ is the carbon concentration in LCs, R is the ideal gas constant, and ∇C and ∇v represent the carbon concentration gradient and the potential gradient as a result of pressure gradient, respectively, which were approximated as:

$$\nabla c \approx \frac{C_V^\theta - C_V^0}{\lambda/2} \quad (9)$$

$$\nabla v \approx \frac{W}{\lambda/2} \quad (10)$$

where λ is the width of a fully developed LAB, and W is the elastic strain energy for precipitating unit amount of carbide. However, the model by Buchwald et al. requires a temperature range of 200 °C–300 °C to reach the experimentally observed LC growth rate, which is unrealistic for normal RCF tests.

Later, Ponzlonsky et al. [65] argued dislocation annihilation to be the driving force for the outflow of carbon from ferrite bands to LCs. By analysing the carbon flux created by carbon release during dislocation annihilation, they gave the expression for calculating the number of cycles for fully developed WEBs (N_b) as:

$$N_b = \frac{\lambda^2 \dot{N}}{D} \quad (11)$$

Compared with the model by Buchwald et al., the model by Ponzlonsky yields a WEB formation rate closer to the experimental observation; however, the model contains numerous bold approximations and is unable to account for the progression of WEB or LC formation.

The latest numerical model for LC thickening was proposed by Fu et al. [55] based on dislocation-assisted carbon migration. Similar to the description of carbon redistribution in

WEM and DERs, the growth of LCs were depicted by a carbon flux equilibrium equation and a carbon mass conservation equation:

$$\frac{d l_{LC}}{d N} (C_V^\theta - C_V^b) \dot{N} = J_d \quad (12)$$

$$\lambda C_V^0 = l_{LC} C_V^\theta + (\lambda - l_{LC}) C_V^b \quad (13)$$

where C_V^b is the carbon concentration in ferrite bands, which is also C_V^l in J_d . This model was proven to accurately predict the experimental results by Buchwald et al. [58], Martin et al. [87] and Fu et al. [55]. The model was also employed by Abdullah et al. [59] to describe the LC thickness evolution under a very high contact pressure (6 GPa) and high operation temperatures (100 °C and 160 °C) to yield accurate predictions.

In addition, Laithy et al. [66] analysed the progressive increase of area covered by WEBS in martensitic and bainitic bearing steels tested under various RCF conditions and proposed a semi-empirical model to describe the formation of both LABs and HABs. The model can produce reasonable predictions but lacks insight into the physics of WEB formation due to its statistical nature. Furthermore, some key input parameters of the model were obtained by fitting to a limited type of experimental data, and therefore it is uncertain whether the model can be extended to other RCF scenarios. Nonetheless, the semi-empirical model is currently the only model that quantifies the formation of HABs.

4. Future Perspectives

Despite a large number of studies on RCF-related microstructural alterations in bearing steels in the literature, some issues of experiment and modelling should be noticed. One of the biggest challenges in the field of RCF is the extremely long testing time. Normal bearings are designed to run for years, and such a time span is unacceptable for common scientific research. In order to reduce the data collection time, accelerated RCF tests with increased contact loads have been widely adopted. However, it is questionable whether the experimental data obtained from these accelerated RCF tests can reflect real bearing performance.

Under appropriate bearing operation conditions, the contact pressures should not exceed the yield strength of material, usually below 2 GPa [21]. However, the most commonly used contact pressures in accelerated RCF tests were 3–4 GPa [46,49,58], which definitely triggered plastic deformation. In some reported cases, the contact pressures even reached as high as 5–6 GPa [14,62].

This is equivalent to conducting a work hardening processing on the material. As the response of bearing steels is dominated by applied load [60], the observed microstructural alterations in accelerated RCF tests may stem from totally different mechanisms compared to those in real bearings. Hence, it is necessary to evaluate the effectiveness of RCF data in the literature by carefully checking the testing conditions, especially when choosing modelling mechanisms.

Nonetheless, RCF-related microstructural alterations in bearing steels continue to be a research hotspot. This is due to the existence of numerous unsolved key questions and paradoxes. In this respect, several important and interesting research directions are suggested for future efforts.

White etching areas and white etching cracks are definitely of the greatest interest to the bearing industry as they are the most relevant microstructural features for unpredictable bearing failures [33]. Sufficient characterisation work has been accomplished thus far to reveal the nature of the microstructure in WEM, and thus any further characterisation of WEM will not lead to fundamental breakthroughs or revolutionary understandings. More attention should be paid to describing and modelling the formation process of WEAs and WECs based on such a large amount of experimental findings. In this respect, several key questions are waiting to be answered.

- The appearance of a symmetric pair of butterflies with reversed over-rolling directions strongly indicates the role played by surface traction. Hence, the question arises as to whether surface traction is the root cause for the initiation of butterflies. If so, does it mean that, under a pure rolling condition, butterflies can be eliminated? In addition, how does surface traction act on butterfly initiation? Although surface sliding can increase the magnitude of subsurface shear stress, this is apparently not the sole mechanism operating, as four-wing-butterflies would be otherwise produced by increasing contact pressure, which is not the case. More work should be done to compare the butterfly formation behaviours under various rolling/sliding conditions.
- Still regarding the symmetry of WEAs and WECs, why does WEM usually appear on only one side or biased towards one side of a crack? If crack surface rubbing is the cause for WEM formation, then according to the law of 'action and reaction forces' the two sides of a crack should have an equal form of WEM, which does not happen. Hence, there must be a factor causing such asymmetry, which remains undetermined. This question can be approached via analysing the difference in stress state within rubbing and rubbed bodies.
- What exactly is the relationship between a growing crack and its adjacent WEM? Despite the emerging knowledge that cracks and WEM exhibit mutual promotion behaviour, stronger experimental evidence is required to prove this point. More attention is also suggested to be paid to the qualitative and quantitative description of the effect of WEM on the crack growth rate, which determines the contact fatigue life.

Dark etching regions manifest the decay of martensitic matrix in bearing steels. The latest understanding of DER formation mechanism is dislocation-assisted carbon migration from the matrix towards pre-existing carbide precipitates [47,53]. In this respect, the following aspects are suggested for future research.

- The applicability of the DER formation model proposed by Fu et al. [47] to various types of parent matrix needs to be further studied. As the inputs of the model strongly depend on the initial microstructure and the plastic response of the material under cyclic loading, more validation work of the model is required. In addition, referring to Liang et al. [71], the effect of hydrogen on DER development can also be incorporated into the model, preferably with experimental validation.
- Under relatively high contact pressures, there exists a competition between work hardening and material softening in DERs, where the former stems from dislocation multiplication and the latter stems from carbon loss in the solid solution. Quantitatively describing the effects of these two competitors is crucial for predicting the evolution of mechanical properties under various testing conditions.
- The impact of DERs on rolling contact fatigue life is still unclear. The key to solving this problem is to reveal the crack initiation and propagation behaviours in DERs where coupling crack formation models with the DER formation mechanism is a reasonable way. Furthermore, the interaction between DERs and WECs/butterflies is a more complex topic to be investigated.

White etching bands may not be of particular interest to the bearing industry as they appear at very late stages of bearing life and thus far there is no evidence showing the relevance between WEBs and bearing failures. Nonetheless, WEBs exhibit a number of interesting paradoxes that are worth studying from a scientific point of view.

- The unique directionality of WEBs, 30° and 80° towards the over-rolling direction is still unexplained. These two inclination angles do not conform to the directions of any stress components under Hertzian contact. It seems that multiple stress components operate simultaneously to cause such directionality. Mere static stress state analysis may be insufficient to tackle this paradox, and the stress history experienced by subsurface material should be taken into consideration. Solving this problem can also shed light on the questions as to the absence of WEBs in symmetric and conjugate directions [65].

- The appearance sequence of high angle and low angle bands needs to be clarified. One possible explanation to this question can be that the magnitude of the responsible stress component for LABs is higher than for HABs, and therefore, under the same rolling contact conditions, the number of stress cycles required to form HABs is higher. Again, in order to confirm this, the corresponding responsible stress components for LABs and HABs must be confirmed first.
- The formation mechanisms of LABs and HABs are still unclear. Although both types of WEBs show significant plastic deformation in ferrite bands, they differ not only in directionality but also in shape. The fact that LABs are thin and HABs are thick suggests different local straining behaviours of the material that need to be studied separately. A relevant question would be what the limiting factor dominating the thickening of LABs and HABs is. This requires more detailed characterisation on these two types of WEBs.

Light etching regions are a type of microstructural transitions that have not been sufficiently studied. Nonetheless, the formation manner of LERs is quite similar to that of DERs. Hence, the corresponding key questions are proposed following the research mode of DERs.

- What is the criterion for LER formation? As LERs only appear in certain types of bearing steels (M50 and M50-NiL), what is the decisive factor for the type of matrix decay during RCF, DERs, LERs or nil?
- What is the nature of LERs? More characterisation work at the nano-scale and the atomic scale is needed to answer this key question. The origin of the white contrast should be investigated by taking into consideration the dislocation behaviour. The detected hardness increase in LERs is also associated with possible dislocation rearrangement.
- Does carbon play a role in LER formation? As one of the most important alloying elements in bearing steels, carbon along with its redistribution dominates the formation of WEM, DERs and LCs. In the case of LERs, the effect of carbon needs to be clarified as well. Therefore, more characterisation work focusing on the distribution of carbon in LERs at the atomic scale, such as atom probe tomography, should be conducted.
- How do cracks initiate and propagate with the presence of LERs? The changes in the microstructure and mechanical properties in LERs definitely affect fatigue crack formation. Solving this problem is the key to associating LERs to RCF life.

5. Concluding Remarks

A general understanding regarding rolling contact fatigue-induced microstructural alterations in bearing steels has been acquired. We reviewed the phenomenology and formation mechanisms of four types of major microstructural features, WEAs/WECs, DERs, LABs/HABs and LERs, with a grasp of the key information in the literature. The prediction of these microstructural alterations is an important aspect in this field, and hence the classical and state-of-the-art models were introduced and analysed. Based on the current progress of research, several key questions and paradoxes regarding each type of microstructural features were raised, suggesting possible future research directions. The main remarks of this review are concluded as follows:

1. WEAs and WECs are of the most research interest to the bearing industry as they are directly associated with bearing failures. The characterisation of WEM is sufficient, while future work is suggested to focus on describing and modelling the formation process of WEAs and WECs.
2. WEM microstructure resembles that caused by SPD, which is driven by crack surface rubbing; however, the unsymmetrical appearance of WEM remains unexplained.
3. Fatigue cracks and their decorating WEM may develop mutually. The previous opinion that WEM is simply a symptom of crack growth is challenged, although stronger experimental evidence is required.
4. DERs manifest the decay of the martensitic matrix dominated by dislocation-driven carbon redistribution.

5. The static stress state alone cannot explain the directionality of WEBs. Solving this problem is also necessary for tackling the paradoxes as to the absence of WEBs in symmetric and conjugate directions.
6. LERs have been insufficiently investigated. More characterisation work at the nano-scale and the atomic-scale is needed to reveal the microstructural nature and the corresponding formation mechanism. The research methodology may follow that of DERs.
7. A dislocation-assisted carbon migration mechanism has been applied to the formation of WEM, DERs and LABs. The input parameters of the theory depend highly upon the initial microstructure and material response to the applied load, which determine the prediction accuracy of the derived models.
8. Hydrogen accelerates the occurrence and development of WEAs/WECs, DERs and WEBs by enhancing dislocation mobility, which can be quantified by considering the HELP mechanism.

Author Contributions: Funding acquisition and writing—review and editing, H.Y.; Writing—review and editing, D.L., Y.W., P.Z. and G.Z. Writing—original draft preparation, H.F. All authors have read and agreed to the published version of the manuscript.

Funding: This research was funded by China Academy of Railway Sciences Corporation Limited (2020YJ148) and National Natural Science Foundation of China (51971011).

Institutional Review Board Statement: Not applicable.

Informed Consent Statement: Not applicable.

Data Availability Statement: Not applicable.

Acknowledgments: H.F. is grateful to Wu Wu for the fruitful discussions.

Conflicts of Interest: The authors declare no conflict of interest. The funders had no role in the design of the study; in the collection, analyses, or interpretation of data; in the writing of the manuscript. The funders approved the publication of the results.

Abbreviations

The following abbreviations are used in this manuscript:

RCF	Rolling contact fatigue
WEAs	White etching areas
WECs	White etching cracks
WEM	White etching matter
DERs	Dark etching regions
WEBs	White etching bands
LABs	Low angle bands
HABs	High angle bands
LCs	Lenticular carbides
LERs	Light etching regions
SEM	Scanning electron microscopy
TEM	Transmission electron microscopy
SPD	Severe plastic deformation
HELP	Hydrogen-enhanced local plasticity

References

1. Fu, H.; Rivera-Díaz-del Castillo, P.E.J. Approaches to model structural and contact fatigue. In *Encyclopedia of Materials: Metals and Alloys*; Caballero, F.G., Ed.; Elsevier: Oxford, UK, 2022; pp. 576–588.
2. Slack, T.S.; Raje, N. A Review of Rolling Contact Fatigue. *J. Tribol.* **2009**, *131*, 041403.
3. Johnson, K. *Contact Mechanics*; Cambridge University Press: Cambridge, UK, 1987.
4. Sackfield, A.; Hills, D.A.; Nowell, D. *Mechanics of Elastic Contacts*; Elsevier: Amsterdam, The Netherlands, 2013.
5. Warhadpande, A.; Sadeghi, F.; Evans, R.D. Microstructural Alterations in Bearing Steels under Rolling Contact Fatigue Part 1—Historical Overview. *Tribol. Trans.* **2013**, *56*, 349–358. [[CrossRef](#)]

6. Tanaka, A.; Furumura, K.; Ohkuma, T. Highly Extended Life of Transmission Bearings of “Sealed-Clean” Concept. *SAE Trans.* **1983**, *92*, 878–889.
7. Furumura, K.; Murakami, Y.; Abe, T. Development of long life bearing steel for full film lubrication and for poor and contaminated lubrication. *Motion Control* **1996**, *1*, 30–36.
8. Fu, H.; Rivera-Díaz-del Castillo, P.E.J. A unified theory for microstructural alterations in bearing steels under rolling contact fatigue. *Acta Mater.* **2018**, *155*, 43–55. [[CrossRef](#)]
9. Gould, B.; Demas, N.G.; Pollard, G.; Rydel, J.J.; Ingram, M.; Greco, A.C. The effect of lubricant composition on white etching crack failures. *Tribol. Lett.* **2019**, *67*, 1–14. [[CrossRef](#)]
10. Fu, H.; Rivera-Díaz-del Castillo, P.E. Evolution of white etching bands in 100Cr6 bearing steel under rolling contact-fatigue. *Metals* **2019**, *9*, 491. [[CrossRef](#)]
11. Jones, A. Metallographic observations of ball bearing fatigue phenomena. In *Symposium on Testing of Bearings*; ASTM International: Buffalo, NY, USA, 1947.
12. El Laithy, M.; Wang, L.; Harvey, T.J.; Vierneusel, B.; Correns, M.; Blass, T. Further understanding of rolling contact fatigue in rolling element bearings—a review. *Tribol. Inter.* **2019**, *140*, 105849. [[CrossRef](#)]
13. Sugino, K.; Miyamoto, K.; Nagumo, M.; Aoki, K. Structural alterations of bearing steels under rolling contact fatigue. *Trans. Iron Steel Inst. Jpn.* **1970**, *10*, 98–111. [[CrossRef](#)]
14. Rydel, J.J.; Toda-Caraballo, I.; Guetard, G.; Rivera-Díaz-del Castillo, P.E.J. Understanding the factors controlling rolling contact fatigue damage in VIM-VAR M50 steel. *Int. J. Fatigue* **2018**, *108*, 68–78. [[CrossRef](#)]
15. Grabulov, A.; Ziese, U.; Zandbergen, H.W. TEM/SEM investigation of microstructural changes within the white etching area under rolling contact fatigue and 3-D crack reconstruction by focused ion beam. *Scripta Mater.* **2007**, *57*, 635–638. [[CrossRef](#)]
16. Vincent, A.; Lormand, G.; Lamagnere, P.; Gosset, L.; Girodin, D.; Dugragne, G.; Fougeres, R. From white etching areas formed around inclusions to crack nucleation in bearing steels under rolling contact fatigue. *Bear. Steels Into 21st Century* **1998**, 1327, 109.
17. Truelove, J.; Blades, L.; Hills, D. Half-plane contact problems in partial slip with varying normal and tangential loads. *Eur. J. Mech.-A/Solids* **2022**, *94*, 104590. [[CrossRef](#)]
18. Alfredsson, B.; Olsson, E. Multi-axial fatigue initiation at inclusions and subsequent crack growth in a bainitic high strength roller bearing steel at uniaxial experiments. *Inter. J. Fatigue* **2012**, *41*, 130–139. [[CrossRef](#)]
19. Evans, M.H. White structure flaking (WSF) in wind turbine gearbox bearings: Effects of ‘butterflies’ and white etching cracks (WECs). *Mater. Sci. Technol.* **2012**, *28*, 3–22. [[CrossRef](#)]
20. Solano-Alvarez, W.; Pickering, E.; Peet, M.; Moore, K.; Jaiswal, J.; Bevan, A.; Bhadeshia, H.K.D.H. Soft novel form of white-etching matter and ductile failure of carbide-free bainitic steels under rolling contact stresses. *Acta Mater.* **2016**, *121*, 215–226. [[CrossRef](#)]
21. Bhadeshia, H.K.D.H. Steels for Bearings. *Prog. Mater. Sci.* **2012**, *57*, 268–435. [[CrossRef](#)]
22. Solano-Alvarez, W.; Bhadeshia, H.K.D.H. White-etching matter in bearing steel. Part II: Distinguishing cause and effect in bearing steel failure. *Metall. Mater. Trans. A* **2014**, *45*, 4916–4931. [[CrossRef](#)]
23. Grabulov, A.; Petrov, R.; Zandbergen, H.W. EBSD investigation of the crack initiation and TEM/FIB analyses of the microstructural changes around the cracks formed under Rolling Contact Fatigue (RCF). *Int. J. Fatigue* **2010**, *32*, 576–583. [[CrossRef](#)]
24. Becker, P.C. Microstructural changes around non-metallic inclusions caused by rolling-contact fatigue of ball-bearing steels. *Met. Technol.* **1981**, *8*, 234–243. [[CrossRef](#)]
25. Evans, M.H.; Walker, J.C.; Ma, C.; Wang, L.; Wood, R.J.K. A FIB/TEM study of butterfly crack formation and white etching area (WEA) microstructural changes under rolling contact fatigue in 100Cr6 bearing steel. *Mater. Sci. Eng. A* **2013**, *570*, 127–134. [[CrossRef](#)]
26. Kang, J.H.; Hosseinkhani, B.; Williams, C.A.; Moody, M.P.; Bagot, P.; Rivera-Díaz-del Castillo, P.E.J. Solute redistribution in the nanocrystalline structure formed in bearing steels. *Scripta Mater.* **2013**, *69*, 630–633. [[CrossRef](#)]
27. Danielsen, H.K.; Guzmán, F.G.; Dahl, K.V.; Li, Y.; Wu, J.; Jacobs, G.; Burghardt, G.; Fæster, S.; Alimadadi, H.; Goto, S.; et al. Multiscale characterization of White Etching Cracks (WEC) in a 100Cr6 bearing from a thrust bearing test rig. *Wear* **2017**, *370*, 73–82. [[CrossRef](#)]
28. Li, Y.J.; Herbig, M.; Goto, S.; Raabe, D. Atomic scale characterization of white etching area and its adjacent matrix in a martensitic 100Cr6 bearing steel. *Mater. Charact.* **2017**, *123*, 349–353. [[CrossRef](#)]
29. Mayweg, D.; Morsdorf, L.; Li, Y.; Herbig, M. Correlation between grain size and carbon content in white etching areas in bearings. *Acta Mater.* **2021**, *215*, 117048. [[CrossRef](#)]
30. Curd, M.E.; Burnett, T.L.; Fellowes, J.; Donoghue, J.; Yan, P.; Withers, P.J. The heterogenous distribution of white etching matter (WEM) around subsurface cracks in bearing steels. *Acta Mater.* **2019**, *174*, 300–309. [[CrossRef](#)]
31. Curd, M.E.; Burnett, T.L.; Fellowes, J.; Yan, P.; Withers, P.J. Redistribution of carbon caused by butterfly defects in bearing steels. *Acta Mater.* **2020**, *183*, 390–397. [[CrossRef](#)]
32. López-Uruñuela, F.J.; Fernández-Díaz, B.; Pagano, F.; López-Ortega, A.; Pinedo, B.; Bayón, R.; Aguirrebeitia, J. Broad review of “White Etching Crack” failure in wind turbine gearbox bearings: Main factors and experimental investigations. *Inter. J. Fatigue* **2021**, *145*, 106091. [[CrossRef](#)]
33. Lai, J.; Stadler, K. Investigation on the mechanisms of white etching crack (WEC) formation in rolling contact fatigue and identification of a root cause for bearing premature failure. *Wear* **2016**, *364*, 244–256. [[CrossRef](#)]

34. Gould, B.; Greco, A.; Stadler, K.; Xiao, X. An analysis of premature cracking associated with microstructural alterations in an AISI 52100 failed wind turbine bearing using X-ray tomography. *Mater. Des.* **2017**, *117*, 417–429. [[CrossRef](#)]
35. Errichello, R.; Budny, R.; Eckert, R. Investigations of bearing failures associated with white etching areas (WEAs) in wind turbine gearboxes. *Tribol. Trans.* **2013**, *56*, 1069–1076. [[CrossRef](#)]
36. Evans, M.H.; Richardson, A.D.; Wang, L.; Wood, R.J.K. Effect of hydrogen on butterfly and white etching crack (WEC) formation under rolling contact fatigue (RCF). *Wear* **2013**, *306*, 226–241. [[CrossRef](#)]
37. Evans, M.H.; Wang, L.; Jones, H.; Wood, R.J.K. White etching crack (WEC) investigation by serial sectioning, focused ion beam and 3-D crack modelling. *Tribol. Inter.* **2013**, *65*, 146–160. [[CrossRef](#)]
38. Evans, M.H.; Richardson, A.; Wang, L.; Wood, R.; Anderson, W. Confirming subsurface initiation at non-metallic inclusions as one mechanism for white etching crack (WEC) formation. *Tribol. Inter.* **2014**, *75*, 87–97. [[CrossRef](#)]
39. Kadin, Y.; Sherif, M.Y. Energy dissipation at rubbing crack faces in rolling contact fatigue as the mechanism of white etching area formation. *Inter. J. Fatigue* **2017**, *96*, 114–126. [[CrossRef](#)]
40. Morsdorf, L.; Mayweg, D.; Li, Y.; Diederichs, A.; Raabe, D.; Herbig, M. Moving cracks form white etching areas during rolling contact fatigue in bearings. *Mater. Sci. Eng. A* **2020**, *771*, 138659. [[CrossRef](#)]
41. Su, Y.S.; Li, S.X.; Yu, F.; Lu, S.Y.; Wang, Y.G. Revealing the shear band origin of white etching area in rolling contact fatigue of bearing steel. *Inter. J. Fatigue* **2021**, *142*, 105929. [[CrossRef](#)]
42. Averbek, S.; Priestersbach, D.; Kerscher, E. Mechanism of fine granular area and white etching crack formation in AISI 52100 bearing steel. *Theor. Appl. Fract. Mech.* **2020**, *108*, 102664. [[CrossRef](#)]
43. Lojkowski, W.; Djahanbakhsh, M.; Bürkle, G.; Gierlotka, S.; Zielinski, W.; Fecht, H.J. Nanostructure formation on the surface of railway tracks. *Mater. Sci. Eng. A* **2001**, *303*, 197–208. [[CrossRef](#)]
44. Baumann, G.; Zhong, Y.; Fecht, H. Comparison between nanophase formation during friction induced surface wear and mechanical attrition of a pearlitic steel. *Nanostruct. Mater.* **1996**, *7*, 237–244. [[CrossRef](#)]
45. Takahashi, J.; Kawakami, K.; Ueda, M. Atom probe tomography analysis of the white etching layer in a rail track surface. *Acta Mater.* **2010**, *58*, 3602–3612. [[CrossRef](#)]
46. Swahn, H.P.C.O.; Becker, P.C.; Vingsbo, O. Martensite decay during rolling contact fatigue in ball bearings. *Metall. Trans. A* **1976**, *7*, 1099–1110. [[CrossRef](#)]
47. Fu, H.; Song, W.; Galindo-Nava, E.I.; Rivera-Díaz-del Castillo, P.E.J. Strain-induced martensite decay in bearing steels under rolling contact fatigue: Modelling and atomic-scale characterisation. *Acta Mater.* **2017**, *139*, 163–173. [[CrossRef](#)]
48. Abdullah, M.U.; Khan, Z.A.; Kruhoeffler, W. Evaluation of dark etching regions for standard bearing steel under accelerated rolling contact fatigue. *Tribol. Inter.* **2020**, *152*, 106579. [[CrossRef](#)]
49. Bush, J.J.; Grube, W.L.; Robinson, G.H. Microstructural and residual stress changes in hardened steel due to rolling contact. *Trans. ASM* **1961**, *54*, e412.
50. Lund, T. Structural alterations in fatigue-tested ball bearing steel. *Jernkontorets Ann.* **1969**, *153*, 337–343.
51. Šmeljova, V.; Schwedt, A.; Wang, L.; Holweger, W.; Mayer, J. Electron microscopy investigations of microstructural alterations due to classical Rolling Contact Fatigue (RCF) in martensitic AISI 52100 bearing steel. *Inter. J. Fatigue* **2017**, *98*, 142–154. [[CrossRef](#)]
52. Kang, J.H.; Kim, J.; Kang, J.Y.; Kwon, S.W.; Kang, M.W.; Hong, S.H. Multiscale study on the dark-etching region due to rolling contact fatigue of 0.57 C-bearing steel. *Acta Mater.* **2022**, *226*, 117666. [[CrossRef](#)]
53. Kang, J.H.; Hosseinkhani, B.; Vegter, R.H.; Rivera-Díaz-del Castillo, P.E. Modelling dislocation assisted tempering during rolling contact fatigue in bearing steels. *Inter. J. Fatigue* **2015**, *75*, 115–125. [[CrossRef](#)]
54. Cottrell, A.H.; Bilby, B.A. Dislocation theory of yielding and strain ageing of iron. *Proc. Phys. Soc. Sect. A* **1949**, *62*, 49. [[CrossRef](#)]
55. Fu, H.; Galindo-Nava, E.; Rivera-Díaz-del Castillo, P.E.J. Modelling and characterisation of stress-induced carbide precipitation in bearing steels under rolling contact fatigue. *Acta Mater.* **2017**, *128*, 176–187. [[CrossRef](#)]
56. El Laithy, M.; Wang, L.; Harvey, T.J.; Vierneusel, B. Re-investigation of dark etching regions and white etching bands in SAE 52100 bearing steel due to rolling contact fatigue. *Inter. J. Fatigue* **2020**, *136*, 105591. [[CrossRef](#)]
57. El Laithy, M.; Wang, L.; Harvey, T.J.; Schwedt, A.; Vierneusel, B.; Mayer, J. White Etching Bands Formation Mechanisms due to Rolling Contact Fatigue. *Acta Mater.* **2022**, *232*, 117932. [[CrossRef](#)]
58. Buchwald, J.; Heckel, R. An analysis of microstructural changes in 52100 steel bearings during cyclic stressing (Microstructural changes in 52100 steel bearing inner rings during cyclic stressing, obtaining thickening rate data on white-etching regions and lenticular carbides). *ASM Trans. Q.* **1968**, *61*, 750–756.
59. Abdullah, M.U.; Khan, Z.A.; Kruhoeffler, W.; Blass, T.; Vierneusel, B. Development of white etching bands under accelerated rolling contact fatigue. *Tribol. Inter.* **2021**, *164*, 107240. [[CrossRef](#)]
60. Voskamp, A.P. Material response to rolling contact loading. *J. Tribol.* **1985**, *107*, 359–366. [[CrossRef](#)]
61. Kocks, U.; Mecking, H. Physics and phenomenology of strain hardening: The FCC case. *Prog. Mater. Sci.* **2003**, *48*, 171–273. [[CrossRef](#)]
62. Kirsch, M.; Trivedi, H. Microstructural Changes in Aerospace Bearing Steels under Accelerated Rolling Contact Fatigue Life Testing. In *Bearing Steel Technologies: 11th Volume, Advances in Steel Technologies for Rolling Bearings*; ASTM International: West Conshohocken, PA, USA, 2017.
63. Ganti, S.; Turner, B.; Kirsch, M.; Anthony, D.; McCoy, B.; Trivedi, H.; Sundar, V. Three-dimensional (3D) analysis of white etching bands (WEBs) in AISI M50 bearing steel using automated serial sectioning. *Mater. Charact.* **2018**, *138*, 11–18. [[CrossRef](#)]

64. Bhattacharyya, A.; Subhash, G.; Arakere, N. Evolution of subsurface plastic zone due to rolling contact fatigue of M-50 NiL case hardened bearing steel. *Int. J. Fatigue* **2014**, *59*, 102–113. [[CrossRef](#)]
65. Polonsky, I.A.; Keer, L.M. On white etching band formation in rolling bearings. *J. Mech. Phys. Solids* **1995**, *43*, 637–669. [[CrossRef](#)]
66. El Laithy, M.; Wang, L.; Harvey, T.J.; Vierneusel, B. Semi-empirical model for predicting LAB and HAB formation in bearing steels. *Inter. J. Fatigue* **2021**, *148*, 106230. [[CrossRef](#)]
67. Pritz, L.; Marsoner, S.; Ebner, R.; Fluch, R.; Tatschl, A.; Münzer, R. Investigation into microstructural changes due to the rolling contact fatigue of the AISI M50 bearing steel. *WIT Trans. Eng. Sci.* **2015**, *91*, 35–45.
68. Arakere, N.K.; Subhash, G. Work hardening response of M50-NiL case hardened bearing steel during shakedown in rolling contact fatigue. *Mater. Sci. Technol.* **2012**, *28*, 34–38. [[CrossRef](#)]
69. Allison, B.; Subhash, G.; Arakere, N.; Haluck, D.A.; Chin, H. Influence of initial residual stress on material properties of bearing steel during rolling contact fatigue. *Tribol. Trans.* **2014**, *57*, 533–545. [[CrossRef](#)]
70. Szost, B.; Rivera-Díaz-del Castillo, P.E.J. Unveiling the nature of hydrogen embrittlement in bearing steels employing a new technique. *Scripta Mater.* **2013**, *68*, 467–470. [[CrossRef](#)]
71. Liang, X.; Rivera-Díaz-del Castillo, P.E.J. Hydrogen-accelerated white etching area formation in bearings under rolling contact fatigue. *Inter. J. Fatigue* **2022**, *159*, 106753. [[CrossRef](#)]
72. Endo, T.; Dong, D.; Imai, Y.; Yamamoto, Y. Study on rolling contact fatigue in hydrogen atmosphere—improvement of rolling contact fatigue life by formation of surface film. In *Tribology and Interface Engineering Series*; Elsevier: Amsterdam, The Netherlands, 2005; Volume 48, pp. 343–350.
73. Uyama, H.; Yamada, H.; Hidaka, H.; Mitamura, N. The effects of hydrogen on microstructural change and surface originated flaking in rolling contact fatigue. *Tribol. Online* **2011**, *6*, 123–132. [[CrossRef](#)]
74. Oezel, M.; Schwedt, A.; Janitzky, T.; Kelley, R.; Bouchet-Marquis, C.; Pullan, L.; Broeckmann, C.; Mayer, J. Formation of white etching areas in SAE 52100 bearing steel under rolling contact fatigue—Influence of diffusible hydrogen. *Wear* **2018**, *414*, 352–365. [[CrossRef](#)]
75. Kürten, D.; Khader, I.; Raga, R.; Casajús, P.; Winzer, N.; Kailer, A.; Spallek, R.; Scherge, M. Hydrogen assisted rolling contact fatigue due to lubricant degradation and formation of white etching areas. *Eng. Failure Anal.* **2019**, *99*, 330–342. [[CrossRef](#)]
76. Kino, N.; Otani, K. The influence of hydrogen on rolling contact fatigue life and its improvement. *JSAE Rev.* **2003**, *24*, 289–294. [[CrossRef](#)]
77. Robertson, I.M.; Birnbaum, H.K.; Sofronis, P. Hydrogen effects on plasticity. *Dislocat. Solids* **2009**, *15*, 249–293.
78. Holweger, W.; Schwedt, A.; Rumpf, V.; Mayer, J.; Bohnert, C.; Wranik, J.; Spille, J.; Wang, L. A Study on Early Stages of White Etching Crack Formation under Full Lubrication Conditions. *Lubricants* **2022**, *10*, 24. [[CrossRef](#)]
79. Vegter, R.H.; Slycke, J.T. The Role of Hydrogen on Rolling Contact Fatigue Response of Rolling Element Bearings. *J. ASTM Int.* **2009**, *7*, 1–12.
80. Imai, Y.; Endo, T.; Dong, D.; Yamamoto, Y. Study on rolling contact fatigue in hydrogen environment at a contact pressure below basic static load capacity. *Tribol. Trans.* **2010**, *53*, 764–770. [[CrossRef](#)]
81. Wranik, J.; Holweger, W.; Lutz, T.; Albrecht, P.; Reichel, B.; Wang, L. A Study on Decisive Early Stages in White Etching Crack Formation Induced by Lubrication. *Lubricants* **2022**, *10*, 96. [[CrossRef](#)]
82. Holweger, W.; Wolf, M.; Merk, D.; Blass, T.; Goss, M.; Loos, J.; Barteldes, S.; Jakovics, A. White etching crack root cause investigations. *Tribol. Trans.* **2015**, *58*, 59–69. [[CrossRef](#)]
83. Pape, F.; Terwey, J.T.; Wiesker, S.; Averbek, S.; Muhmann, C.; Lipinsky, D.; Arlinghaus, H.F.; Kerscher, E.; Sauer, B.; Poll, G. Tribological research on the development of white etching cracks (WECs). *Forsch. Ingenieurwes.* **2018**, *82*, 341–352. [[CrossRef](#)]
84. Dogahe, K.J.; Guski, V.; Mlikota, M.; Schmauder, S.; Holweger, W.; Spille, J.; Mayer, J.; Schwedt, A.; Görlach, B.; Wranik, J. Simulation of the Fatigue Crack Initiation in SAE 52100 Martensitic Hardened Bearing Steel during Rolling Contact. *Lubricants* **2022**, *10*, 62. [[CrossRef](#)]
85. Takemura, H.; Matsumoto, Y.; Murakami, Y. Development of a new life equation for ball and roller bearings. *SAE Trans.* **2000**, *109*, 261–267.
86. Park, J.; Lee, K.; Kang, J.H.; Kang, J.Y.; Hong, S.; Kwon, S.W.; Lee, M.G. Hierarchical microstructure based crystal plasticity-continuum damage mechanics approach: Model development and validation of rolling contact fatigue behavior. *Inter. J. Plast.* **2021**, *143*, 103025. [[CrossRef](#)]
87. Martin, J.A.; Borgese, S.F.; Eberhardt, A.D. Microstructural alterations of rolling—Bearing steel undergoing cyclic stressing. *J. Basic Eng.* **1967**, *89*, 932–942. [[CrossRef](#)]